#### Cover Page



### Universiteit Leiden



The handle <a href="http://hdl.handle.net/1887/26921">http://hdl.handle.net/1887/26921</a> holds various files of this Leiden University dissertation

Author: Doan, Nhat Trung

Title: Quantitative analysis of human brain MR images at ultrahigh field strength

Issue Date: 2014-06-17

## 2

# Texture analysis of ultrahigh field T<sub>2</sub>\*-weighted MR images of the brain: application to Huntington's disease

This chapter was adapted from:

**N. T. Doan**, S. J. A. van den Bogaard, E. M. Dumas, A. G. Webb, M. A. van Buchem, R. A. C. Roos, J. van der Grond, J. H. C. Reiber, and J. Milles, "Texture analysis of ultrahigh field  $T_2^*$ -weighted MR images of the brain: application to Huntington's disease," *Journal of Magnetic Resonance Imaging*, vol. 39, no. 3, pp. 633–640, 2014.

#### Abstract

**Purpose**: To develop a framework for quantitative detection of between-group textural differences in ultrahigh field  $T_2^*$ -weighted MR images of the brain.

**Materials and methods**: MR images were acquired using a three-dimensional (3D)  $T_2^*$ -weighted gradient echo sequence on a 7 Tesla MRI system. The phase images were high-pass filtered to remove phase wraps. Thirteen textural features were computed for both the magnitude and phase images of a region of interest based on 3D Gray-Level Co-occurrence Matrix, and subsequently evaluated to detect between-group differences using a Mann-Whitney U-test. We applied the framework to study textural differences in subcortical structures between premanifest Huntington's disease (HD), manifest HD patients, and controls.

**Results**: In premanifest HD, four phase-based features showed a difference in the caudate nucleus. In manifest HD, 7 magnitude-based features showed a difference in the pallidum, 6 phase-based features in the caudate nucleus, and 10 phase-based features in the putamen. After multiple comparison correction, significant differences were shown in the putamen in manifest HD by two phase-based features (both adjusted p values = 0.04).

**Conclusion**: This study provides the first evidence of textural heterogeneity of subcortical structures in HD. Texture analysis of ultrahigh field  $T_2^*$ -weighted MR images can be useful for noninvasive monitoring of neurodegenerative diseases.

#### Introduction 2.1

Recent technological developments of clinical ultrahigh field MR scanners have enabled the acquisition of data with increased image resolution, signal-to-noise ratio and contrastto-noise ratio [31]. In particular,  $T_2^*$ -weighted imaging has recently received much attention due to its capability to characterize tissue magnetic susceptibility [26, 68, 69] and phase images showing an increased sensitivity to small differences in tissue susceptibility with higher field strengths [26]. T<sub>2</sub>-weighted images have been used in quantitative studies of the brain at lower fields, e.g. as an indirect means to study iron in subcortical structures of patients with multiple sclerosis and clinically isolated syndromes [70, 71]). With ultrahigh field MRI, T<sub>2</sub>-weighted images have been examined qualitatively for improved visualization of anatomical structures such as the cerebral cortex [72] and the hippocampus [27]. However, approaches for the extraction and utilization of quantitative information from these images have not yet been fully explored. In phase-based studies [70, 71, 73], the mean phase value of a region of interest (ROI) is often used. This measure does not consider any spatial relationships between phase voxels and as a result does not reflect local spatial differences. Apart from global phase shifts, additional local changes among image voxels such as focal or distributed alterations within the ROI cannot be captured by the mean phase value. This limitation can be overcome by means of texture analysis.

Image texture describes the spatial arrangement of visual patterns that relate to intuitive notions such as coarseness, contrast and smoothness. Texture analysis techniques allow one to mathematically quantify the textural aspect of images independently of the way they are perceived by the human eye. In the literature, several texture analysis approaches have been proposed such as transform-based approaches, signal processing approaches and statistical approaches [35]. Gray-Level Co-occurrence Matrix (GLCM) [41] is one of the most widely used approaches because of its ability to characterize image properties based on voxel spatial correspondence. Based on this approach, 3D GLCMs, which yield features with higher discriminative power compared to 2D GLCMs [42], can be computed and subsequently used to derive second-order textural features. The added value of texture analysis in disease monitoring has been demonstrated in MR-based studies of neurodegenerative diseases such as Alzheimer's disease [49] and Parkinson's disease [61]. This tool can potentially be used to quantitatively study changes reflected on ultrahigh field T<sub>2</sub>\*-weighted images.

Huntington's disease (HD) is a slowly progressive neurodegenerative disease clinically characterized by symptoms of motor, behavioral, psychiatric and cognitive dysfunction [6]. Global and localized atrophy in subcortical structures has been reported in HD [18, 21]. Additionally, studies have shown profound cellular deterioration in the putamen and caudate nucleus based on histological data [74-76] and increased iron accumulation in the same structures using MRI [22]. Abnormal iron levels in the basal ganglia have been demonstrated both post mortem [77] and in vivo using T<sub>2</sub> relaxometry [78-80]. We hypothesized that indications of change at tissue level in subcortical structures in HD, possibly related to iron accumulation, can be captured using texture analysis of ultrahigh field T<sub>2</sub>\*-weighted images.

In this work, we propose a quantitative framework composed of 7 Tesla (T) T<sub>2</sub><sup>\*</sup>weighted imaging and the GLCM texture analysis approach which allows one to capture between-group differences. We apply the proposed framework to study textural hetero-

TABLE 2.1: Subject characteristics.

	Premanifest HD	Manifest HD	Controls
Age	$43.7 \pm 9.9$	$51.5 \pm 12.2$	$48.1 \pm 1.3$
CAG repeat	$43.7 \pm 3$	$43.8 \pm 3.2$	n/e
Gender (male/female)	3/4	5/3	3/2

n/e = not examined

geneity in subcortical structures of subjects with premanifest and manifest HD and healthy controls. Furthermore, by means of texture analysis, we aim to study the quantitative values of ultrahigh field  $T_2^*$ -weighted images.

#### 2.2 Materials and methods

#### 2.2.1 Subjects

Twenty participants were recruited from our institution's neurology outpatient clinic, of which 7 were premanifest HD gene carriers, 8 manifest HD patients and 5 controls. Inclusion criteria for the premanifest HD consisted of a positive genetic test for a CAGrepeat expansion of > 39 in the Htt-gene, an absence of motor abnormalities defined as a score of  $\leq 5$  on the Unified Huntington's Disease Rating Scale (UHDRS), total motor score (TMS) and a diagnostic confidence level of 0 or 1 on the UHDRS. Inclusion criteria for manifest HD consisted of a positive genetic test for a CAG-repeat expansion of > 39 in the Htt-gene, a presence of motor abnormalities defined as a score of > 5 on the UHDRS-TMS and a diagnostic confidence level of 4 on the UHDRS. Healthy gene negative family members or spouses were recruited as controls. Exclusion criteria for all participants consisted of significant (neurological) comorbidity, claustrophobia and MRI incompatibility. The study was approved by the Medical Ethical Committee. All participants gave written informed consent. Characteristics of the participants are presented in Table 2.1.

#### 2.2.2 MR acquisition

The participants underwent MRI scanning on a 3T and a 7T Philips whole body systems (Philips Healthcare, Best, the Netherlands) within 24 h.  $T_1$ -weighted images were acquired on both scanners and a  $T_2^*$ -weighted imaging sequence was performed on the 7T scanner. Texture analysis was performed on the 7T  $T_2^*$ -weighted images. The 3T  $T_1$ -weighted images were used for automated segmentation of subcortical structures while the 7T  $T_1$ -weighted images were only used for registration purpose. The following scan parameters were applied:

3T T<sub>1</sub>-weighted MRI

 $T_1$ -weighted image volumes were acquired using a 3D gradient echo acquisition sequence with the following imaging parameters: repetition time (TR) = 7.7 ms, echo time (TE) = 3.5 ms, flip angle (FA) =  $8^{\circ}$ , field-of-view (FOV) = 240 x 224 x 224 mm<sup>3</sup>, 164 sagittal slices to cover the entire brain, voxel size 1.1 x 1.0 x 1.0 mm<sup>3</sup>.

7T T<sub>1</sub>-weighted MRI

A 3D gradient echo sequence was applied with the following parameters: TR = 18 ms, TE = 8.9 ms,  $FA = 8^{\circ}$ , FOV 210 x 169 x 120 mm<sup>3</sup>, voxel size 0.3 x 0.3 x 2.0 mm<sup>3</sup>.

7T T<sub>2</sub>-weighted MRI

A high-resolution 3D heavily  $T_2^*$ -weighted gradient echo sequence was used with the following parameters: TR = 24 ms, TE = 15 ms, FA = 45°, FOV 220 x 182 x 142 mm<sup>3</sup>, voxel size 0.25 x 0.25 x 0.5 mm<sup>3</sup>.

Examples of the acquired images are shown in Figure 2.1.

#### 2.2.3 Overall framework

Image analysis was performed as follows. First, preprocessing included intensity inhomogeneity correction for the magnitude images, phase unwrapping for the phase images, and segmentation of the subcortical structures using the 3T  $T_1$ -weighted images. After preprocessing, rigid registration was applied to align all images of each subject to the subject 3T  $T_1$ -weighted space. Subcortical segmentations were performed using the 3T  $T_1$ -weighted images and the segmentation masks were then used to identify subcortical structures in the 7T  $T_2^*$ -weighted magnitude and phase images. Subsequently, thirteen Haralick features [41] were computed for both 7T  $T_2^*$ -weighted magnitude and phase images of each structure based on a GLCM. A nonparametric statistical testing was then performed on each Haralick feature to compare the premanifest and manifest groups with a control group.

#### 2.2.4 Image processing

#### 2.2.4.1 Intensity inhomogeneity correction

Intensity non-uniformity is a common artifact in MR imaging characterized by anatomically independent intensity variation throughout the data. Correction for this artifact is crucial as it degrades the performance of quantitative MRI analysis [81]. In this study, we applied the N3 algorithm [82] for the correction of the 7T  $T_1$ -weighted and 7T  $T_2$ -weighted magnitude images using its implementation in MIPAV software [83].

#### 2.2.4.2 Phase unwrapping

The phase of each pixel in the MR image, reconstructed on the scanner, is bound to the interval of  $[-\pi,\pi]$ . However, its actual range is much larger due to the intrinsic inhomogeneity of the magnetic field, resulting in phase wraps in the images. In this study, phase wrap removal, also referred to as phase unwrapping, was performed based on high-pass filtering in the k-space as implemented in Wang et al. [25].

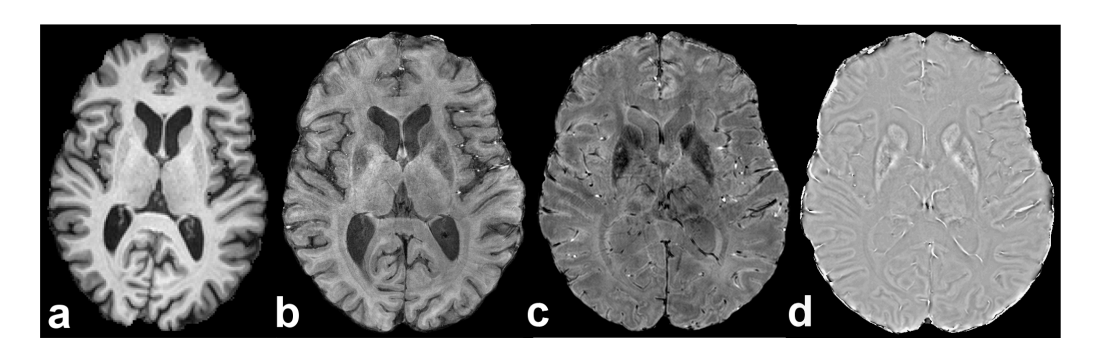


FIGURE 2.1: Examples of 3T  $T_1$ -weighted magnitude (a), 7T  $T_1$ -weighted magnitude (b), 7T  $T_2^*$ -weighted magnitude (c), and 7T  $T_2^*$ -weighted (unwrapped) phase (d) images.

#### 2.2.4.3 Segmentation of subcortical structures

Texture analysis on subcortical nuclei requires segmentation of these structures. To obtain segmentation of the subcortical nuclei, we applied FIRST [84], part of the FSL package, on the 3T  $T_1$ -weighted images. The software has also been successfully applied in recent HD studies [20–22]. The resulting subcortical masks were used to segment subcortical structures on the 7T  $T_2^*$ -weighted magnitude and phase images. In the present work, we studied the following structures: amygdala, caudate nucleus, hippocampus, pallidum, putamen and thalamus.

#### 2.2.4.4 Registration

Subcortical segmentation on 7T  $T_2^*$ -weighted magnitude and phase images using the 3T  $T_1$ -based subcortical masks required registration to transform 7T  $T_2^*$ -weighted images to the 3T  $T_1$ -weighted space. Since the accuracy of direct registration between 7T  $T_2^*$ -weighted and 3T  $T_1$ -weighted images suffered from the differences in type of MR sequences and field strengths, the 7T  $T_1$ -weighted images were used in an intermediate step during the registration to improve the overall performance of registration. The registration was done using the *elastix* registration package [85] in two steps: rigid body registration of 7T  $T_2^*$ -weighted images to 7T  $T_1$ -weighted images using mutual information as the similarity measure and a B-spline interpolator, followed by rigid body registration of 7T  $T_1$ -weighted images to 3T  $T_1$ -weighted images using correlation ratio and a B-spline interpolator.

After registration, since the computation of 3D textural features in this study required isotropic data, all subcortical segmentations were resampled from  $1.1 \times 1.0 \times 1.0 \text{ mm}^3$  to  $1.0 \times 1.0 \times 1.0 \text{ mm}^3$ .

#### 2.2.5 Texture computation

#### 2.2.5.1 3D Gray-Level Co-occurrence Matrix

In this study, the textural features were computed based on 3D Gray-Level Co-occurrence Matrix (GLCM). A GLCM M of an image I represents how often every combination of gray scale values occurs in the image at a given spatial offset. The matrix is constructed by systematically searching the whole image and tabulating the frequency of different gray level combinations. Each entry M(i,j) of the matrix is equal to the number of times voxel I(x,y,z), with value i, and voxel  $I(x+\Delta_x,y+\Delta_y,z+\Delta_z)$ , with value j, occur in the image. I(x,y,z) and  $I(x+\Delta_x,y+\Delta_y,z+\Delta_z)$  are termed neighboring voxels. The coordinate of the neighbor of a voxel being considered is identified by a displacement vector (or offset)  $\overrightarrow{\Delta}(\Delta_x,\Delta_y,\Delta_z)$ . This displacement vector is composed of the distance between the voxels and the direction in which they are searched for.

Mathematically, M(i, j) is computed as:

$$M(i,j) = \sum_{x=1}^{P} \sum_{y=1}^{Q} \sum_{z=1}^{L} \begin{cases} 1, & \text{if } I(x,y,z) = i \text{ and } I(x+\Delta_x, y+\Delta_y, z+\Delta_z) = j \\ 0, & \text{otherwise} \end{cases}$$
 (2.1)

where P, Q, and L are the image dimensions. To avoid obtaining a sparse GLCM, image intensity is often quantized to a smaller range of N gray levels. In this study, we used a global intensity quantization scheme to preserve the relative difference in dynamic range between subjects. For each structure of interest, the global maximum intensity  $I_{max}$  and global minimum intensity  $I_{min}$  over all studied subjects were computed and the quantization step defined as  $q = \frac{I_{max} - I_{min}}{N-1}$ . Quantization of the data pertaining to the

structure of interest was performed for every subject using the resulting global dynamic range and quantization step. All GLCMs were square matrices of dimension N computed from the quantized images. This global scheme has been reported to be optimal compared to a local scheme that scales each individual dynamic range to the same range of [1; N][42]. In this work, we chose a commonly used value of N of 32 gray levels [35] for intensity quantization. Prior to this intensity quantization step, the dynamic range of the whole-brain magnitude images was scaled to the same range of [0;1023] (10 bits) for intensity normalization.

Since there is no evidence for pathological differences between the different hemispheres in HD, we did not investigate the left and right sub-structures separately, but rather combined them together. The GLCM for the whole structure was computed as follows. Prior to the computation of GLCM, the 3D volume of each structure was oriented such that it was symmetrical with respect to the y = 0 plane. At a given offset specified by the displacement vector of  $(\Delta_x, \Delta_y, \Delta_z)$ , one GLCM was computed for the left structure using this vector and another GLCM was computed for the right structure using a modified version of the displacement vector  $(\Delta_x, -\Delta_y, \Delta_z)$ . The sum of the two GLCMs was the GLCM computed for the whole structure.

In this 3D computation of GLCM, we considered 13 directions and a distance of 1 voxel. For each structure, one GLCM was computed for each direction, resulting in 13 GLCMs. These 13 GLCMs were then averaged to obtain a non-directional GLCM.

#### 2.2.5.2 Haralick features

Thirteen Haralick features [41] were derived from each GLCM after its normalization. One GLCM was computed for each structure, resulting in 13 features being computed for each structure. These features included: angular second moment  $(f_1)$ , contrast  $(f_2)$ , correlation  $(f_3)$ , sum of squares  $(f_4)$ , inverse difference moment  $(f_5)$ , sum average  $(f_6)$ , sum variance  $(f_7)$ , sum entropy  $(f_8)$ , entropy  $(f_9)$ , difference variance  $(f_{10})$ , difference entropy  $(f_{11})$ , information measure of correlation 1  $(f_{12})$  and information measure of correlation 2  $(f_{13})$ . Some of the features intuitively represent image texture properties. Figure 2.2 presents an illustrative example which shows the values of 4 Haralick features computed from simple synthetic textures. Angular second moment measures the uniformity of the image. A higher value of angular second moment indicates less variation in the image intensity. Its value ranges from 0 (image D with randomly-distributed intensity) to 1 (image A with constant intensity). Contrast quantifies the local variations in the image with a higher value of contrast indicating higher intensity differences between a voxel and its neighbors over the whole image. For example, image C shows very sharp local black-white transitions which are represented by a very high value of contrast of this texture compared to other textures which show less local intensity variation. Correlation, ranging from -1 to 1, measures linear dependencies of image gray-levels. Image C for example shows a high linear dependence which is not present in image D. Such differences are captured by the difference in the computed values of correlation feature (note that the correlation of a constant image (image A) is not defined). Entropy is a measure of disorder or randomness. It takes higher values for more complex images, for instance, image B and D have higher entropy compared to image A and C. For details about the formulae used to compute each Haralick feature, we refer the readers to the original reference in the field [41].

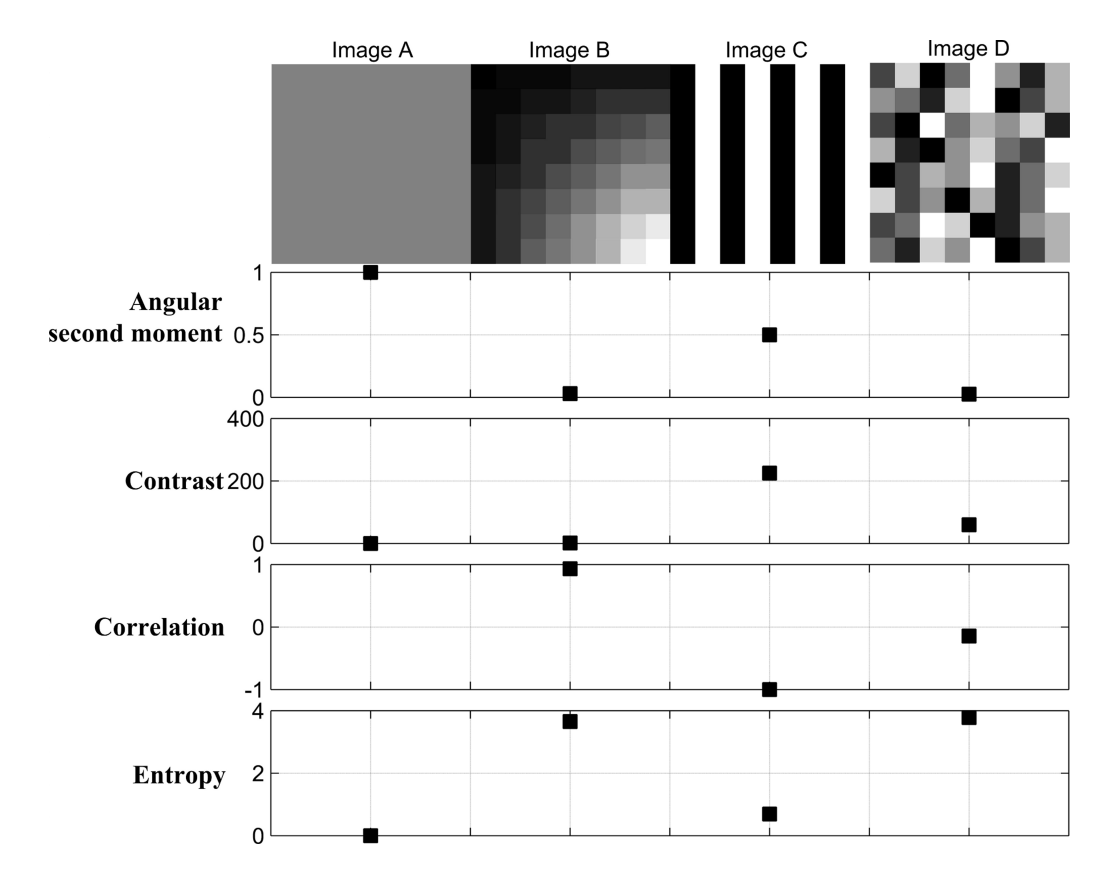


FIGURE 2.2: Illustrative example of 4 Haralick features (angular second moment, contrast, correlation and entropy) computed from synthetic images. Each image (**A-D**) presents a simple texture. A GLCM was computed for each image using a displacement vector of  $\pm (0,1)$  pixel and a quantization level N of 16.

#### 2.2.6 Statistical testing

After feature computation, a Mann-Whitney U-test [86] was applied in the following two comparisons: premanifest HD versus controls, and manifest HD versus controls. The Mann-Whitney U-test, a non-parametric test which makes no assumption about normal distribution of the data, was used to determine whether the mean of two groups are significantly different from each other. In each of the aforementioned comparisons, for each structure, 13 Mann-Whitney U-tests were carried out for the 13 Haralick features. Subsequently, to check whether the differences shown by the Mann-Whitney U-tests were significant, we performed a correction for multiple comparisons as follows. The Bonferroni procedure was applied to adjust the resulting 13 p values. The adjusted p values were then compared to the significance level to accept or reject the null hypothesis of equal means between groups. Both feature computation and statistical tests, with significance level of 0.05, were carried out in Matlab (Mathworks, Natick, MA, version 7.13).

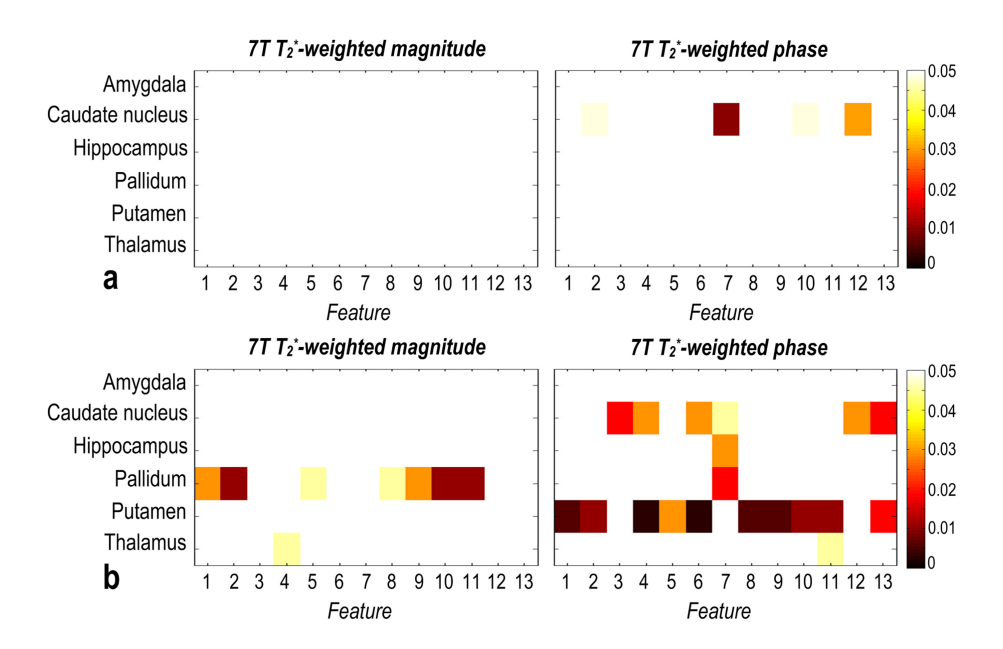


FIGURE 2.3: p values of the Mann-Whitney U-tests before correction for multiple comparisons: premanifest HD versus controls (a); manifest HD versus controls (b). In each case, the results of the tests performed for each studied structure using either 7T T<sub>2</sub>-weighted magnitude features or 7T  $T_{\nu}^{z}$ -weighted phase features are presented. p values smaller or equal to 0.05 were color-coded such that the darker the color, the smaller the value.

#### Results 2.3

This section presents the results of the statistical tests performed to compare the premanifest HD group and manifest HD group with the control group. For each subcortical structure, a total of 26 features were computed from 7T T<sub>2</sub>\*-weighted data, 13 using the magnitude images and 13 using the phase images. In each comparison, the results obtained before and after correcting the p values for 13 features are presented. For the differences revealed by the Mann-Whitney U-tests before the correction, Figure 2.3 presents the resulting p values and Table 2.2 provides a detailed list of the discriminative features. After correction for multiple comparisons, statistically significant differences were found in the putamen between manifest HD and controls. Further details are presented as follows.

#### 2.3.1 Premanifest HD versus Controls

When evaluating the discriminative power of each feature individually, no correction for multiple comparisons was applied. The magnitude-based features did not show statistically significant differences. Four phase-based features including the sum variance, information measure of correlation 1, contrast, and difference variance showed differences in the caudate nucleus (p = 0.01, 0.03, 0.048, and 0.048 respectively). When a more stringent significance level was applied using the Bonferroni procedure, none of the differences shown by the phase-based features were significant.

TABLE 2.2: List of features showing differences when comparing premanifest and manifest HD groups with the control group. The listed features were found based on the p values obtained before the correction for multiple comparisons. Asterisks indicate features that showed significant difference after correction for multiple comparisons.

	Comparison	Structure	Discriminative feature
T <sub>2</sub> *-weighted magnitude	Manifest HD vs. Controls	Pallidum	Angular second moment $(f_1)$
		Pallidum	Contrast $(f_2)$
		Pallidum	Inverse difference moment $(f_5)$
		Pallidum	Sum entropy $(f_8)$
		Pallidum	Entropy $(f_9)$
		Pallidum	Difference variance ( $f_{10}$ )
		Pallidum	Difference entropy $(f_{11})$
		Thalamus	Sum of squares $(f_4)$
T <sub>2</sub> -weighted phase	Premanifest HD vs. Controls	Caudate nucleus	Contrast $(f_2)$
		Caudate nucleus	Sum variance $(f_7)$
		Caudate nucleus	Difference variance ( $f_{10}$ )
		Caudate nucleus	Information measure of correlation 1 ( $f_{12}$ )
	Manifest HD vs. Controls	Caudate nucleus	Correlation $(f_3)$
		Caudate nucleus	Sum of squares $(f_4)$
		Caudate nucleus	Sum average $(f_6)$
		Caudate nucleus	Sum variance $(f_7)$
		Caudate nucleus	Information measure of correlation 1 ( $f_{12}$ )
		Caudate nucleus	Information measure of correlation 2 ( $f_{13}$ )
		Hippocampus	Sum variance $(f_7)$
		Pallidum	Sum variance $(f_7)$
		Putamen	Angular second moment $(f_1)$
		Putamen	Contrast $(f_2)$
		Putamen	Sum of squares $(f_4)^*$
		Putamen	Inverse difference moment $(f_5)$
		Putamen	Sum average $(f_6)^*$
		Putamen	Sum entropy $(f_8)$
		Putamen	Entropy $(f_9)$
		Putamen	Difference variance ( $f_{10}$ )
		Putamen	Difference entropy ( $f_{11}$ )
		Putamen	Information measure of correlation 2 ( $f_{13}$ )
		Thalamus	Difference entropy $(f_{11})$

#### 2.3.2 Manifest HD versus Controls

As illustrated in Figure 2.3, before correction for multiple comparisons, 7 of 13  $T_2^*$ -weighted magnitude-based features showed a difference in the pallidum (0.011  $\leq p \leq$  0.045). Six of 13 and 10 of 13  $T_2^*$ -weighted phase-based features showed a difference in the caudate nucleus (0.019  $\leq p \leq$  0.045) and the putamen (0.003  $\leq p \leq$  0.03), respectively. The magnitude-based features are mainly discriminative in the pallidum, whereas the phase-based features are mainly discriminative in the caudate nucleus and the putamen. In addition, one magnitude-based feature and one phase-based feature showed a difference in the thalamus (sum of squares with p = 0.045 for magnitude and difference entropy with p = 0.045 for phase). The sum variance computed from the phase images showed a difference in the hippocampus (p = 0.03) and the pallidum (p = 0.019). No features showed differences in the amygdala. After correction for multiple comparisons, significant differences were shown in the putamen by two phase-based features (sum of squares and sum average, both with adjusted p value of 0.04).

#### Discussion

We have presented a novel framework for quantitative detection of textural heterogeneity in subcortical structures and between-group differences using 7T T<sub>2</sub>\*-weighted images and a second-order texture analysis approach. We evaluated the framework on in vivo data of premanifest HD gene carriers, manifest HD patients and control subjects. The results provide the first evidence of textural heterogeneity of subcortical structures in HD. Importantly, the regional specific textural differences are in line with structural deficits previously reported in vivo and ex vivo in both premanifest and manifest HD [16, 87].

In the presented framework, several preprocessing steps were performed prior to textural computation. Two of them, inhomogeneity correction and phase unwrapping, were a prerequisite to further analysis and performed on different data, the former on 7T magnitude images and the latter on phase images. Two other steps were due to the need to identify regions of interest on 7T T<sub>2</sub><sup>\*</sup>-weighted images: subcortical structure segmentation on 3T T<sub>1</sub>-weighted images and registration from 7T T<sub>2</sub>\*-weighted space to 3T space. Textural computation itself involved two steps, GLCM computation and derivation of Haralick features, which are standard steps in GLCM-based texture analysis. The only steps that may affect texture analysis are the registration of T<sub>2</sub>\*-weighted images to 3T space and resampling to 1mm<sup>3</sup> isotropic voxels for computation of 3D textural features. In our view, these particular two steps may tend to reduce textural differences with data presenting other contrasts rather than exacerbating them. Finally, this type of processing is in line with existing literature on texture analysis.

Resolutions of the 3T T<sub>1</sub>-weighted images and the 7T images were different, which may constrain the outcome results to a lower resolution than that of original T<sub>2</sub>\*-weighted image data. However, it should be noted that the different data were used for different purposes. First, 3T T<sub>1</sub>-weighted data were used for automated segmentation of regions of interest. Both 3T and 7T T<sub>1</sub>-weighted data were used to align the 3T-based regions of interest on 7T T<sub>2</sub>\*-weighted data in 3T space. A high order B-Spline interpolator was used during the transformation to minimize the effect of image interpolation. Second,  $T_2^*$ -weighted image data were used for texture analysis in the aligned regions of interest. For the computation of 3D textural features, those data were resampled to isotropic data of 1 x 1 x 1 mm<sup>3</sup>, a resolution at which texture analysis of brain MR images is typically performed. The GLCM-based approach we used, which is solely based on voxel pairs, is not likely to be affected by the variation in spatial resolution during processing since it captures many different aspects of texture, and thus enabling the derived features to reflect image textures across different resolutions.

Textural features were computed based on GLCMs. In this computation, a GLCM matrix is normalized by dividing it by the sum of all entries [41], effectively normalizing the matrix for volume differences. Due to this normalization, differences in volume between the groups due to atrophy are not expected to cause a confounding effect in the findings of this study. Moreover, the magnitude-based features and phase-based features, computed from the same structures, yielded statistical differences for different structures, which would not be the case if structure size were a confounder.

GLCMs of each structure were averaged across directions. In general, one may consider treating GLCMs computed from different directions separately. However, in this work, we evaluated the framework using images of subcortical structures and assumed that textures would be approximately isotropic in these structures. We carried out experiments

to compare the features computed from GLCMs following different directions. A similar pattern of p values was obtained, empirically confirming our assumption. In addition, this pattern was similar to that obtained using the averaged GLCM. Based on this result, we chose to use the averaged GLCMs in computing the Haralick features.

The proposed framework revealed differences in subcortical structures in HD. Differences were found, before correcting the p values for multiple comparisons, mostly in the caudate, the putamen, and the pallidum in the manifest stage. Four phase-based features showed differences in the caudate nucleus in the premanifest stage. Among these four discriminative features, sum variance and information measure of correlation 1 showed differences in both premanifest and manifest stages. This signifies a possibility of using them to track textural changes in the caudate nucleus. Contrast and difference variance did not show a difference when comparing manifest HD with controls, which might be explained by the cross-sectional characteristic of the study. When considering Haralick features as a whole, significant differences were found after correction for multiple comparisons in the putamen between manifest and control groups using phase-based features. This supports the hypothesis that there is a textural change in the putamen observed in the manifest stage of the disease and this change could be detected using 7T  $T_2^*$ -weighted phase images. Investigators have reported atrophy in the caudate nucleus, the putamen [88, 89], the pallidum [20] in both premanifest and manifest stages, and the thalamus in the manifest stage of HD [90]. The textural findings of our study concur with existing findings on structural changes in these structures in the manifest stage, especially the putamen where significant differences were found.

It is known that the contrast on  $T_2^*$ -weighted images is induced by magnetic susceptibility of paramagnetic substances such as iron-containing ferritin [91]. This contrast is dominated by the tissue susceptibility effects at high field strengths [31]. There is increasing evidence that iron is involved in pathomechanisms that underlie many neurodegenerative diseases [14]. We speculate that the differences in texture shown in this study are related to abnormal iron deposition patterns which could be linked to altered axonal transport of iron and the effects of possible myelin breakdown [78]. Further evidence of increased iron in HD, especially in the putamen, comes from another study using asymmetric spin echo sequences [22] which reported increased iron content in the manifest and not in the premanifest stage. If iron is the main contributor to textural differences, then significant results are more likely to be found in manifest HD than in premanifest HD. The significant differences found in the comparison between manifest HD and controls provide supportive data for a causal role of iron in the textural changes reflected by 7T  $T_2^*$ -weighted phase images.

In the context of this study, 7T  $T_2^*$ -weighted features are sensitive to between-group differences with the phase-based features being more sensitive than the magnitude-based features. This indicates that 7T  $T_2^*$ -weighted images could be used for quantitative studies of textural changes inside structures. In addition, the results obtained using the 7T  $T_2^*$ -weighted phase images are different from those using the 7T  $T_2^*$ -weighted magnitude images, suggesting that they may have different information content. Finally, although the proposed texture analysis framework uses 7T  $T_2^*$ -weighted scans, it could also be applied to  $T_2^*$ -weighted scans obtained with a clinical 3T MRI system.

In conclusion, we have developed an automated framework for detecting between-group textural differences using 7T  $T_2^*$ -weighted imaging and a second-order texture analysis approach. The results obtained from in vivo HD data show that textural

differences can be detected using the proposed framework. We report the first evidence of textural heterogeneity of subcortical structures in HD and we show that the phase-based features are more sensitive than the magnitude-based features. Texture analysis of ultrahigh field  $T_2^*$ -weighted MR images could provide useful textural measures for noninvasive disease monitoring.

#### 2.5 Acknowledgement

The 3D  $T_1$ -weighted MRI Images were acquired via the TRACK-HD study. We would like to thank the TRACK-HD study team for their support. TRACK-HD is supported by the CHDI/High Q Foundation, a not for profit organization dedicated to finding treatments for Huntington's disease.